ACKNOWLEDGMENTS

This work is supported partially by the Young Scholar Foundation of Nanjing University of Science & Technology, the Excellent Young Teachers Program of Moe, PRC, and the Natural Science Foundation of China under contract no. 60271005.

REFERENCES

1. S.D. Gedney and L. Hamilton, Full-wave CAD-based design of a finite ground CPW directional filter, Int J RF and Microwave CAE 10 (2000), 308–318.
2. H.-H. Wu and Y.-J. Chan, High-Q inductors and low-loss band-pass filters on Al_2O_3 substrates, Thin-film Technol Lett 20 (1999), 322–326.
3. G.D. Alley, Interdigital capacitors and their application to lumped-element microwave integrated circuits, IEEE Trans Microwave Theory Techn 18 (1970), 1028–1033.
4. J.L. Hobdell, Optimization of interdigital capacitors, IEEE Trans Microwave Theory Techn 27 (1979), 788–791.
5. I. Kneppo and J. Fabian, Microwave integrated circuits, Chapman & Hall, London.
6. M. Naghed and I. Wolff, Equivalent capacitances of coplanar waveguide discontinuities and interdigitated capacitors using a three-dimensional finite difference method, IEEE Trans Microwave Theory Techn 38 (1990), 1808–1815.
7. S.S. Gevorgian, T. Martinsson, P.L.J. Linner, and E.L. Kollberg, CAD models for multilayered substrate interdigital capacitors, IEEE Trans Microwave Theory Techn 44 (1996), 896–904.
8. Lei Zhu and Ke Wu, Corrections to "Accurate circuit model of interdigital capacitor and its application to design of new quasi-lumped miniaturized filters with suppression of harmonic resonance, IEEE Trans Microwave Theory Techn 50 (2002), 2412–2413.
9. J.W. Bandler, R.M. Biernacki, Shao Hua Chen, D.G. Swanson, Jr., and Shen Ye, Microstrip filter design using direct EM field simulation, IEEE Trans Microwave Theory Techn 42 (1994), 1353–1359.
10. A. Sutono, D. Heo, Y.J. Emery Chen, and J. Laskar, High-Q LTCC-based passive library for wireless system-on-package (SOP) module development, IEEE Trans Microwave Theory Techn 49 (2001), 1715–1724.
11. Gregory L. Creech and Bradley J. Paul, Artificial neural networks for fast and accurate EM-CAD of microwave circuits, IEEE Trans Microwave Theory Techn 45 (1997), 794–802.
12. P.M. Waston and K.C. Gupta, EM-ANN Models for Microstrip vias and interconnects in dataset circuits, IEEE Trans Microwave Theory Techn 44 (1996), 2495–2503.
13. B.Z. Wang and J.S. Hong, Artificial neural network models for the discontinuities in stripline circuits, International Journal Infrared and Millimeter Waves 21 (2000), 677–688.
14. Anand Veluswami and Michel S. Nakhla, The application of NN to EM-based simulation and optimization of interconnects in high-speed VLSI, IEEE Trans Microwave Theory Techn 45 (1997), 712–723.
15. Howard Demuth and Mark Beale, Neural Network Toolbox for use with Matlab, User's Guide, the Mathworks, Inc., Natick, MA, 1994.
16. F.D. Foresee and M.T. Hagan, Gauss–Newton approximation to Bayesian regularization, Proc Int Joint Conf on Neural Networks, 1997, pp. 1930–1935.
17. Daniel S. Weile and Eric Michielssen, Genetic algorithm optimization applied to electromagetics: A Review, IEEE Trans Antennas Propagate 45 (1997), 343–353.

ANTENNA-COUPLED VOx THIN-FILM MICROBOLOMETER ARRAY

F. J. González, M. Abdel-Rahman, and G. D. Boreman
School of Optics/CREOL
University of Central Florida
4000 Central Florida Blvd.
Orlando, FL 32816-2700

Received 17 January 2003

ABSTRACT: *Two-dimensional arrays of log-periodic antenna-coupled microbolometers were fabricated using VOx and Nb thin films as bolometric materials, which have different temperature coefficients of resistance. Noise, response, and angular characteristics of both types of microbolometer arrays were measured and compared. VOx-based devices presented a 4.5× better response and 5.5× better signal-to-noise ratio than Nb-based devices. Radiation patterns show that a further increase in response can be obtained by better matching the VOx bolometer to the antenna elements.* © 2003 Wiley Periodicals, Inc. Microwave Opt Technol Lett 38: 235–237, 2003; Published online in Wiley InterScience (www.interscience.wiley.com). DOI 10.1002/mop.11024

Key words: *microbolometer; vanadium oxide; antenna-coupled detectors*

1. INTRODUCTION

Two-dimensional arrays of antenna-coupled microbolometers are used as fast infrared detectors that can be integrated into commercial readout integrated circuits (ROICs) [1], however, their measured responsivity is lower than the required for commercial infrared imaging applications [2]. The voltage responsivity of a bolometer is given by [3]:

$$\Re_v = \alpha \cdot |Z_{th}| \cdot V_{bias}, \tag{1}$$

where α is the temperature coefficient of resistance of the bolometer, V_{bias} is the dc bias voltage across the device, and Z_{th} is the thermal impedance of the device. The temperature coefficient of resistance (TCR) is the material parameter used to quantify the temperature T dependence of the resistance R of the material and is defined as

$$\alpha = \frac{1}{R}\frac{dR}{dT}. \tag{2}$$

As we can see form Eq. (1), the TCR of the bolometric material is directly proportional to the responsivity of the detector; therefore, the choice of the thin-film heat-sensitive material is an important factor in achieving good response from the microbolometers. A thin films of sputtered Nb, which has a TCR close to $0.003K^{-1}$, was used as bolometric material in [1]. Vanadium is a metal with a variable valence forming a large number of oxides which have a very narrow range of stability [4], films of vanadium oxide (VOx) consisting of a mixture of various oxides present a $TCR \approx 0.02K^{-1}$ and have been used in the past to fabricate microbolometers [5]. Films of stoichiometric VO_2 with TCRs greater than $0.05K^{-1}$ and a more involved deposition process have also been reported [6]. In this paper the performance of a VOx-based antenna-coupled microbolometer is evaluated and compared to a Nb-based device.

2. METHOD

Two dimensional arrays of log-periodic-antenna-coupled microbolometers with a 50 μm × 50 μm pixel area were used in this study

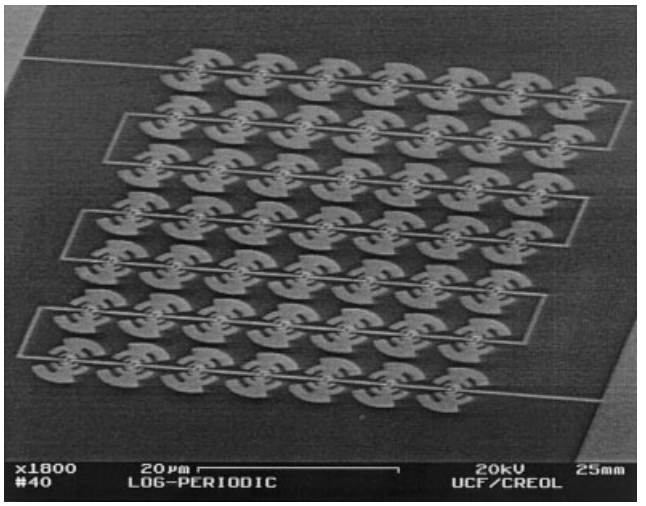

Figure 1 Scanning electron micrograph of a 2D array of log-periodic antenna coupled detectors

(Fig. 1). The antenna arrays were patterned using electron-beam lithography and lift-off at the Cornell Nanofabrication Facility (Ithaca, NY). The antenna elements and the dc bias line that serially connects them are made of 100-nm thick evaporated gold; for every antenna element there is a 0.8 μm $\times$ 0.5 μm patch of bolometric material at the feed. On one set of wafers, 60 nm of VOx was RF-sputtered at 5 mtorr of Argon pressure and on another set of wafers, a 70-nm film of Nb was DC-sputtered. These detectors were all fabricated on 3-in. high-resistivity ($\rho \approx 3000$ Ωcm) Si wafers with 200 nm of thermally grown SiO_2.

The processed wafers were diced into 1 cm^2 chips and bonded into specially made chip carriers. Testing of the devices was done using a CO_2-laser at 10.6 μm focused by an $F/8$ optical train which had an almost diffraction-limited spot with a $1/e^2$ radius of 200 μm and an irradiance of 25 W/cm^2 at the focus. Noise, response, and angular measurements were made on both sets of wafers using the procedure described in [1].

The 2D arrays of microbolometers presented an average dc resistance of 1.2 $\pm$ 0.1 kΩ for the Nb-based detectors and 450 $\pm$ 50Ω for the VOx detectors. The measurements were made at a bias voltage of 300 mV.

3. RESULTS

The response of the antenna arrays to 10.6 μm radiation was measured, and the Nb-based detectors gave a polarization dependent signal of 5.1 $\pm$ 1 μV while the measured response of the VOx-based devices was 22.5 $\pm$ 2.5 μV, which corresponds to a 4.5$\times$ increase in response. Figure 2 shows the noise frequency spectrum measured with an HP3585B spectrum analyzer. The Nb-based devices had a noise voltage spectrum of 54.3 $\pm$ 2.7 nV/$\sqrt{\text{Hz}}$ at 12 kHz, while the VOx-based devices presented a noise voltage spectrum of 44.3 $\pm$ 2.0 nV/$\sqrt{\text{Hz}}$ at the same frequency. This represents a 5.5$\times$ increase in signal-to-noise ratio of the VOx-based devices over the Nb-based ones.

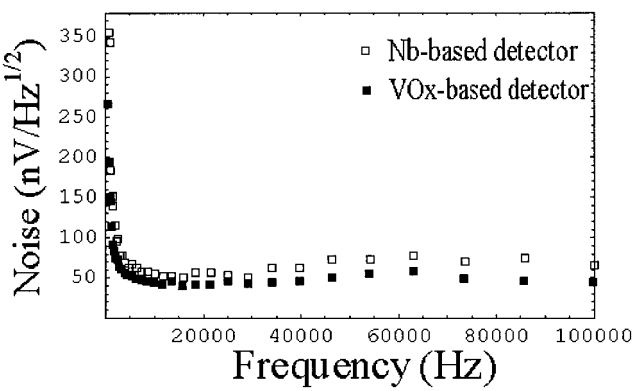

Figure 2 Noise frequency spectrum for Nb- and VOx-based detectors

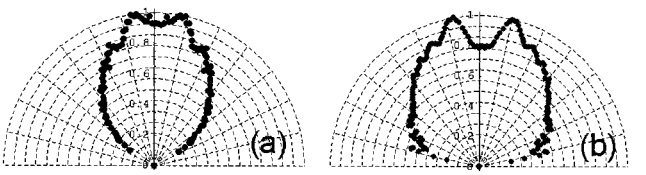

Figure 3 Radiation patterns of (a) Nb-based 2D array, and (b) VOx-based 2D array

Figure 3 shows the measured angular patterns of the Nb-based devices and the VOx based devices, the radiation characteristics for similar antenna array configurations show that the impedance at the feed does alter the electromagnetic characteristics of the antenna array; in this particular case, the Nb-based array presents a more directive pattern than the VOx-based detector, which indicates that the impedance of the Nb patch is a better match for the individual log-periodic elements of the array. The thickness of the VOx bolometer can be varied to better match its impedance to the antenna elements and obtain a further increase in response.

4. CONCLUSIONS

We have measured the response, noise, and radiation patterns of Nb-based and VOx-based 2D arrays of log-periodic antenna-coupled microbolometers. The VOx-based devices present a response 4.5$\times$ higher and a 5.5$\times$ better signal-to-noise ratio than the Nb-based devices. Measured radiation patterns showed that the gain in response and in signal-to-noise ratio can be further increased by better matching the impedance of the bolometric detector to the antenna elements, which would yield an increase in response closer to the 5–10$\times$ expected due to the better TCR of VOx as compared to Nb thin films.

ACKNOWLEDGMENTS

This work was performed in part at the Cornell Nanofabrication Facility (a member of the National Nanofabrication Users Network) which is supported by the National Science Foundation under Grant ECS-9731293, its users, Cornell University and Industrial Affiliates.

This material is based upon research supported by NASA grant no. NAG5-1308.

REFERENCES

1. F.J. González, M.A. Gritz, C. Fumeaux, and G.D. Boreman, Two dimensional array of antenna-coupled microbolometers, Int J Infrared and Millimeter Waves 23 (2002), 785–797.
2. S. Sedky, P. Fiorini, K. Baert, L. Hermans, and R. Mertens, Characterization and optimization of infrared poly SiGe bolometers, IEEE Trans Electron Devices 46 (1999), 675–682.
3. F.J. González, C. Fumeaux, J. Alda, and G.D. Boreman, Thermal impedance model of electrostatic discharge effects on microbolometers, Microwave Optical Technol Lett 26 (2000), 291–293.
4. H. Jerominek, F. Picard, and V. Denis, Vanadium Oxide films for optical switching and detection, Optical Engg 32 (1993), 2092–2099.

5. B.E. Cole, R.E. Higashi, and R.A. Wood, Monolithic two-dimensional arrays of micromachined microstructures for infrared applications, Proc IEEE 86 (1998), 1679–1686.
6. Y.V. Zerov and V.G. Malyarov, Heat-sensitive materials for uncooled microbolometer arrays, J Opt Technol 68, 939–948.

A NOVEL ACCURATE PEEC-BASED 3D MODELING TECHNIQUE FOR RF DEVICES OF ARBITRARY CONDUCTOR-MAGNET STRUCTURE

Haibo Long,[1] Zhenghe Feng,[1] Haigang Feng,[2] and Albert Wang[2]
[1] State Key Lab on Microwave and Digital Communications
Dept. of Electronic Engineering
Tsinghua University
Beijing, 100084, P. R. China
[2] Integrated Electronics Laboratory
Dept. ECE, Illinois Institute of Technology
Chicago, IL 60616

Received 10 January 2003

ABSTRACT: *This paper presents magPEEC, a new 3D electro-magnetic modeling technique that extends the existing PEEC approach to analyze arbitrary conductor-magnet structures by accounting for fictitious magnetized currents on a magnetic material surface. Applications for magnetic-cored/layered spiral inductors demonstrate validity and accuracy of magPEEC. Possible solutions to improve RF IC inductors using magnetic cores are discussed.* © 2003 Wiley Periodicals, Inc.
Microwave Opt Technol Lett 38: 237–240, 2003; Published online in Wiley InterScience (www.interscience.wiley.com). DOI 10.1002/mop.11025

Key words: *partial element equivalent circuits (PEEC); fictitious magnetized currents; magnetic-cored/layered RF IC inductors*

1. INTRODUCTION

Nowadays, magnetic materials have been widely used to make electro-magnetic (EM) devices such as micro electro mechanical systems (MEMS) and on-chip spiral inductors for RF IC applications to improve inductance and quality factor. Inductors using magnetic films operated at multi-GHz frequency have been reported [1]. It is impractical to analyze these structures with magnetic films or cores by using existing full-wave approaches, such as finite-difference or finite-element methods, due to their computational deficiency. The simulation approaches given in [2] and [3] have limited applications due to their 2D nature. A new simulation program called Fastmag, was reported in [4], which can only deal with structures with magnetic materials separated from electrical conductors and is not suitable for true 3D structure simulation due to the equivalent loop-structure mesh cell used. PEEC approach was firstly proposed to model 3D multi-conductor systems in [5], which was later extended to include dielectrics [6]. The PEEC method allows for calculations being reduced to static calculations by neglecting retardation, while still maintaining high accuracy analogous to the full-wave methods [6]. This paper presents a new modeling technique, called magPEEC, which extends the PEEC approach to analyze arbitrary 3D electro-magnetic structures that permits conductors to be outside, touching or inside magnetic materials—a desired feature for modeling many sophisticated electro-magnetic structures.

Contract grant sponsors: National "973" R&D Project of China, grant no. G1999033105; National Natural Science Foundation of China; grant no. 60171015.

ILLUSTRATIONS

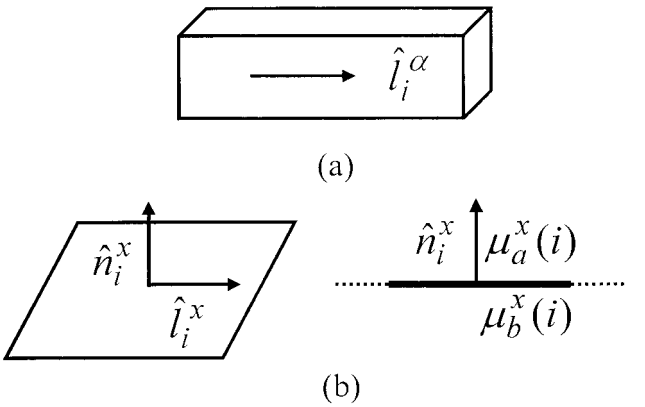

Figure 1 (a) A filament cell in region α; (b) A panel cell in region x (with $x = \beta, \gamma$)

2. magPEEC: MAGNETIC MATERIALS INCLUDED

For an arbitrary 3D EM structure with conductors and magnetic materials, currents are distributed in three regions, that is, conductor bodies carrying bulk currents outside magnetic materials (denoted as region α), conductor-magnet interface carrying surface currents (denoted as region β), and magnetic surfaces carrying surface currents without contacting conductors (denoted as regions γ). By using fictitious magnetized currents on a magnetic material surface, the magnetic problem is equivalent to the free-space problem. The real conductive currents and fictitious magnetic current densities at a point $\bar{r}$ are denoted as $\underline{\bar{J}_c(\bar{r})}$ and $\underline{\bar{J}_f(\bar{r})}$, respectively. The total equivalent current density denoted as $\underline{\bar{J}_t}$ is based on the equation $\underline{\bar{J}_t(\bar{r})} = \underline{\bar{J}_c(\bar{r})} + \underline{\bar{J}_f(\bar{r})}$. For each mesh cell mentioned in this paper, the total through currents through it due to $\underline{\bar{J}_c}$, $\underline{\bar{J}_f}$, and $\underline{\bar{J}_t}$ are denoted as I_c, I_f, and I_t, respectively.

Region α is discretized into N^{α} filament cells, as shown in Figure 1(a). Related parameters for the i^{th} filament cell include current flowing direction $\underline{\hat{l}_i^{\alpha}}$, through electrical voltage V_i^{α}, filament bulk B_i^{α}, current crossing area A_i^{α}, and current flowing length D_i^{α}. Regions β and γ are discretized into N^{β} and N^{r} panel cells, respectively, as shown in Figure 1(b). Related parameters for the i^{th} panel cell in region x (with $x = \beta, \gamma$) include current flowing direction $\underline{\hat{l}_i^x}$, panel's normal direction $\underline{n_i^x}$, through electrical voltage V_i^x, panel area S_i^x, surface current crossing width W_i^x, and current flowing length D_i^x. For convenience, the normal direction is defined as pointing from b side to a side of the panel, as shown in Figure 1(b). $\mu_a^x(i)$ and $\mu_b^x(i)$ are the permeabilities of both sides, with $\mu_{ra}^x(i)$ and $\mu_{rb}^x(i)$ the corresponding relative permeabilities. Current densities over these cells all are assumed locally constant.

Analogous to problems of currents distributed in free space, the magnetic vector potential is obtained as follows: